ORIGINAL ARTICLE

Targeting PFKL with penfluridol inhibits glycolysis and suppresses esophageal cancer tumorigenesis in an AMPK/FOXO3a/BIM-dependent manner

Cancan Zheng[a], Xiaomei Yu[a], Yiyao Liang[b], Yidong Zhu[c], Yan He[c], Long Liao[a], Dingkang Wang[a], Yanming Yang[a], Xingfeng Yin[a], Ang Li[b], Qingyu He[a,*], Bin Li[a,*]

[a]MOE Key Laboratory of Tumor Molecular Biology and Key Laboratory of Functional Protein Research of Guangdong Higher Education Institutes, Institute of Life and Health Engineering, Jinan University, Guangzhou 510632, China
[b]Guangdong Key Laboratory of Non-human Primate Research, Guangdong-Hong Kong-Macau Institute of CNS Regeneration, Key Laboratory of CNS Regeneration, Ministry of Education, Jinan University, Guangzhou 510632, China
[c]MOE Key Laboratory of Tumor Molecular Biology and Guangdong Provincial Key Laboratory of Bioengineering Medicine, National Engineering Research Center of Genetic Medicine, Institute of Biomedicine, College of Life Science and Technology, Jinan University, Guangzhou 510632, China

Abstract As one of the hallmarks of cancer, metabolic reprogramming leads to cancer progression, and targeting glycolytic enzymes could be useful strategies for cancer therapy. By screening a small molecule library consisting of 1320 FDA-approved drugs, we found that penfluridol, an antipsychotic drug used to treat schizophrenia, could inhibit glycolysis and induce apoptosis in esophageal squamous cell carcinoma (ESCC). Gene profiling and Ingenuity Pathway Analysis suggested the important role of AMPK in action mechanism of penfluridol. By using drug affinity responsive target stability (DARTS) technology and proteomics, we identified phosphofructokinase, liver type (PFKL), a key enzyme in glycolysis, as a direct target of penfluridol. Penfluridol could not exhibit its anticancer property in PFKL-deficient cancer cells, illustrating that PFKL is essential for the bioactivity of penfluridol. High PFKL expression is correlated with advanced stages and poor survival of ESCC patients, and silencing of PFKL significantly suppressed

tumor growth. Mechanistically, direct binding of penfluridol and PFKL inhibits glucose consumption, lactate and ATP production, leads to nuclear translocation of FOXO3a and subsequent transcriptional activation of *BIM* in an AMPK-dependent manner. Taken together, PFKL is a potential prognostic biomarker and therapeutic target in ESCC, and penfluridol may be a new therapeutic option for management of this lethal disease.

1. Introduction

Cancer cells exhibit metabolic reprogramming to provide sufficient energy and biosynthesis for cell proliferation, invasion and migration[1]. The phenomenon that tumor cells rely on glycolysis to provide energy is called Warburg effect, which is the main form of metabolic reprogramming in cancer[2]. Based on the metabolic differences between tumor and normal cells, targeting enzymes involved in the glycolytic pathway may offer a therapeutic window to modulate cancer metabolism and suppress cancer progression[3]. Compared with target-based discovery of lead compounds, drug repositioning is a strategy for identifying new indication for existing drugs. Drug repositioning is a growing trend because of its high efficiency, shorter duration of development, low-cost and decreased risk of failure. In this study, by screening a small molecule library consisting of 1320 US Food and Drug Administration (FDA)-approved drugs, we identified penfluridolas a novel anticancer agent. Penfluridol is a first-generation diphenylbutylpiperidine used in clinic for the treatment of schizophrenia. According to our knowledge, the anticancer bioactivity of penfluridol in esophageal cancer and the mechanisms involved remain unknown.

The investigation on the action mechanims of drugs is vital to their clinical implication. In this study, RNA sequencing (RNA-seq) and bioinformatic analysis suggested the involvement of AMP-activated protein kinase (AMPK) signaling in the anticancer effect of penfluridol. As a classical energy sensor, AMPK is activated under conditions of energy stress, when intracellular ATP level declines and intracellular AMP increases, as occurs during nutrient deprivation or hypoxia[4,5]. A great deal of evidence points to a role for AMPK as an inhibitor of tumorigenesis[5], which induces nuclear translocation and transcriptional activation of *FOXO3a*, as well as increased BIM expression[6,7]. Discovery of drugs targeting AMPK/FOXO3a/BIM and the potential as anticancer agent warrant investigation.

Drug affinity response target stability (DARTS) is an efficient method for identifying targets proteins of small molecules. The interaction between small molecules and proteins protects the target proteins from being digested by protease, and then identified by mass spectrometry[8,9]. Here, by using DARTS technology and mass spectrometry-based proteomics, we identified phosphofructokinase, liver type (PFKL) as a direct target of penfluridol. During the first committed step of glycolysis, phosphofructokinase-1 (PFK-1) catalyzes the phosphorylation of fructose 6-phosphate to fructose 1,6-bisphosphate (FBP), which is irreversible[10,11]. Thus, PFK-1 is an important control point in the glycolytic pathway, and this enzyme is widely held to dictate the pace of glycolytic flux. There are three forms of PFK-1 in human, named PFK-M (muscle), PFK-L (liver) and PFK-P (platelet)[12]. Accumulating evidence indicated that PFKL

participated in the development of cancer[3,13,14]. However, whether PFKL contributes to tumorigenesis in esophageal squamous cell carcinoma (ESCC) is unclear.

In this study, by performing gain- and loss-of-function experiments and a series of functional assays, we examined the anticancer property of penfluridol and the functional and clinical significance of PFKL in ESCC. The pharmacological mechanism whether penfluridol suppresses Warburg effect and tumorigenesis through regulation of AMPK/FOXO3a/BIM signaling pathway was investigated.

2. Materials and methods

2.1. Cell culture and drugs

The human ESCC cell lines, KYSE30, KYSE150, KYSE270 were obtained from DSMZ (Braunschweig, Germany), and cultured in RPMI 1640 (Thermo Fisher Scientific, Waltham, MA, USA) supplemented with 10% fetal bovine serum (FBS; ExCell Bio, Shanghai, China) at 37 °C in 5% CO_2. Penfluridol and compound C were obtained from Selleck Chemicals (Huston, TX, USA). The 2-deoxy-D-glucose (2-DG) was obtained from Merck (Burlington, MA, USA).

2.2. Tissue microarray and immunohistochemistry

Immunohistochemistry was performed as described previously[15]. The expression of PFKL was analyzed in the tissue microarray including 206 ESCC tissues and 135 corresponding normal tissues (Shanghai Outdo Biotech, Shanghai, China). In brief, the tissue microarray was incubated with PFKL antibody (1:100 dilution, GeneTex, Alton Pkwy Irvine, CA, USA) overnight at 4 °C followed by corresponding biotinylated secondary antibody. For scoring, each microarray core was categorized into four groups: score 1 (negative), score 2 (weakly positive), score 3 (moderately positive), and score 4 (strongly positive).

2.3. Plasmids, transfection and site-directed mutagenesis

The coding sequence of human PFKL was cloned into pcDNA3.1 vector (Transheep, Shanghai, China). The mutant#1 construct with mutaions in Thr-193 and Gln-197, the mutant#2 construct with mutaions in Asp-226, Arg-253 and Leu-257, and the mutant#3 construct with mutaions in His-453 and Ala-456, were created using the Fast Mutagenesis System (TransGen Biotech, Beijing, China). The plasmids were transfected into ESCC cells by Lipofectamine 3000 (Thermo Fisher Scientific), and transfection and establishment of stable cell lines were performed as previously described[16]. Wild-type and mutant *BIM*

promoter were cloned into pGL3 vector (Promega, Madison, WI, USA), respectively. Small interference RNAs (siRNAs) against *FOXO3a* (Transheep) were transfected into KYSE150 and KYSE270 cells by Lipofectamine 3000 (Thermo Fisher Scientific). The sequences of primers for cloning and mutation are listed in Supporting Infromation Table S1, and the sequences of siRNAs for *FOXO3a* are listed in Supporting Inforamtion Table S2.

2.4. Clustered regularly interspaced short palindromic repeats (CRISPR)/CRISPR-associated protein 9 (Cas9) genome editing

The *PFKL*-knockout cell lines were established with CRISPR/Cas9 techonology as previously described[17]. In brief, the pLentiCRISPR/Cas9 V2 vector expressing the sgRNA targeting *PFKL* was transfected into 293T cells, the virus-containing culture supernatant was collected to infect ESCC cells and puromycin was used to select *PFKL*-deficient cells. Successful knockout of *PFKL* was validated by Western blotting and genomic DNA sequencing. The sequences of sgRNA are as followed, sg*PFKL*#1: ACTTACCAGGATCCGGTCGA; sg*PFKL*#2: TTGGCCTTACCTCGTAGATG.

2.5. Cell viability assay

Cell viability was measured according to the manufacturer's instructions[18]. Cells were seeded in a 96-well plate and treated with different treatments of penfluridol. WST-1 (Beyotime, shanghai, China) was added and placed at 37 °C for 1 h, and the absorbance at 450 nm was quantified by an automated microplat spectrophotometer (BioTek Instruments, Winooski, VT, USA).

2.6. Colony formation assay

ESCC cells were seeded in 6-well plates and cultured for two weeks, the cells were washed with phosphate buffered saline (PBS), fixed with methanol for 15 min, then stained with crystal violet (0.1%) for 15 min, and finally counted for analysis.

2.7. Cell apoptosis assay

Cell apoptosis was determined by the Annexin V-FITC/PI Apoptosis Detection Kit (KeyGen, China)[19]. In brief, cells suspended in PBS were stained with Annexin V-FITC and PI for 20 min in dark. Apoptosis was analyzed on a BD Accuri C6 flow cytometer (BD Biosciences, San Diego, CA, USA).

2.8. Seahorse assay

The real-time extracellular acidification rate (ECAR) and oxygen consumption (OCR) were measured using the Seahorse XF Glycolysis Stress Test Kit or Seahorse XF Cell Mito Stress Test Kit on the Seahorse XF 96 Extracellular Flux Analyzer (Seahorse Bioscience, North Billerica, MA, USA) according to the manufacturer's introductions. In brief, 1×10^4 ESCC cells were plated in XF96 cell culture microplates and treated with penfluridol. Glucose, oligomycin, and 2-deoxy-glucose were used to determine ECAR value, whereas oligomycin, carbonyl cyanide-*p*-trifluoromethoxyphenylhydrazone (FCCP), and rotenone were used to measure OCR.

2.9. Measurement of glucose consumption, lactate production and ATP production

Glucose colorimetric/fluoroetric assay kit, D-lactate colorimetric assay kit, ATP assay kit were used to determine glucose consumption, lactate production, and ATP production respectively, according to the manufacturer's protocols (BioVision, Milpitas, CA, USA). In brief, ESCC cells were seeded into 6-well plates and treated with penfluridol for 24 h. After starve and replacement of new medium, the glucose content in the supernatant was determined according to the manufacturer's instructions.

2.10. RNA sequencing (RNA-seq) and ingenuity pathway analysis (IPA)

RNA-seq was performed at the Beijing Genomics Institute Tech (Shenzhen, China). Compared with the control group, the differentially expressed genes (fold change>2.0) were subjected to IPA analysis (Ingenuity Systems, Redwood City, CA, USA) for pathway enrichment.

2.11. Western blotting

Preparation of cell lysates and protocol of Western blotting were described previously[20]. In brief, the mixture of cell lysates and loading buffer was boiled and loaded into sodium dodecyl sulfate polyacrylamide gel for electrophoresis. The protein was transferred to polyvinylidene fluoride membrane, and blocked with 5% fat-free dry milk in Tris-buffered saline Tween-20. After incubation with primary antibody for 1−2 h at room temperature, the membrane was washed with Tris-buffered saline Tween-20 and probed with corresponding horseradish peroxidase-conjugated secondary antibody for 1 h at room temperature. Signals were detected with Clarity Western ECL Substrate Kit (Bio-Rad, Hercules, CA, USA). The primary antibodies used included AMPK (1:1000 dilution), p-AMPK (1:1000 dilution), p-p70S6 (1:1000 dilution), caspase-3 (1:1000 dilution), cleaved caspase-3 (1:300 dilution) and BIM (1:1000 dilution) from Cell Signaling Technology (Beverly, MA, USA), FOXO3a (1:1000 dilution), GAPDH (1:1000 dilution) and Lamin B (1:1000 dilution) from Proteintech (Chicago, IL, USA), actin (1:1000 dilution) from Santa Cruz Biotechnology (Santa Cruz, CA, USA), and PFKL (1:1000 dilution) from GeneTex.

2.12. Immunofluorescence

The immunofluorescence was performed as described previously[21]. Cells were fixed with 4% paraformaldehyde for 10 min and treated with 0.1% Triton-100 for 10 min, then blocked with 5% BSA for 1.5 h. The cells were incubated with the primary antibody against FOXO3a overnight at 4 °C, and then the fluorescent secondary antibody was added at room temperature for 1.5 h. After DAPI counterstaining, the images were collected by laser scanning confocal microscopy.

2.13. Quantitative real-time polymerase chain reaction (qRT-PCR)

Total RNA was extracted using Trizol (Thermo Fisher Scientific) according to the manufacturer's instructions. Reverse transcription was performed using PrimeScript II first Strand cDNA Synthesis Kit (Takara, Dalian, China). Quantitative PCR was performed

using SYBR Premix Ex TaqII (Takara) on a Bio-Rad Mini Opti-con real-time PCR system. The primers used were: 5′-CAA-GAGTTGCGGCGTATTGGAG-3′ (forward) and 5′-ACACCAGGCGGACAATGTAACG-3′ (reverse).

2.14. Dual luciferase reporter assay

The dual luciferase reporter assay was performed according to the manufacturer's instructions[22]. The plasmids expressing the wild-type or mutant *BIM* promoter region were cotransfected into ESCC cells with the pRL-TK (Promega) in presence or absence of penfluridol, and luciferase activity was measured by using a Dual-Luciferase Reporter Assay System (Promega).

2.15. Chromatin immunoprecipitation (ChIP) assay

ChIP assay was carried out by using SimpleChIP Enzymatic Chromatin IP kit (Cell Signaling Technology) according to manufacturer's protocol. In brief, cells were fixed with formaldehyde for protein−DNA corsslinking, followed by sonication. The supernatant was mixed with FOXO3a antibody or negative control IgG antibody, and incubated at 4 °C overnight. ChIP-grade protein G agarose beads were added to each reaction and incubated at 4 °C for 2 h with rotation. After washing, DNA was purified with the elution buffer and subjected to qPCR analysis. The primers used were: 5′-GTGGGGGATGGGCGCGCA-3′ (forward); 5′-CTGGGTTGCCTCCCGCGC-3′ (reverse).

2.16. DARTS assay

Cell lysates were incubated with penfluridol for 30 min at room temperature, followed by proteinase K treatment for 5 min, and terminated with sodium deoxycholate (Sigma−Aldrich, St. Louis, MO, USA). Proteins were identified by mass spectrometry and bioinformatic analyses.

2.17. Mass spectrometry and bioinformatic analyses

Mass spectrometry-based proteomics was performed as previously described[17]. The protein was digested with trypsin, desalted by MonoTIPTM C18 pipette tip (GL Sciences, Tokyo, Japan) and resuspended in anhydrous acetonitrile solution. The peptides were analyzed by Orbitrap Fusion Lumos mass spectrometer (Thermo Fisher Scientific), and Spectronaut software (Omicsolution Co., Ltd., Shanghai, China) was used to analyze the data.

2.18. PFKL activity assay

The activity of PFKL was determined by Phosphofructokinase test kit (Nanjing Jiancheng Bioengineering Institute, Nanjing, China) according to the manufacturer's instructions. ESCC cells were treated with penfluridol for 24 h, and suspended in extract buffer. After centrifuge, the supernatant was applied for activity detection. The absorbance at 340 nm was measured by the microplate spectrophotometer (BioTek Instruments, Winooski, VT, USA).

2.19. FBP assay

FBP assay was carried out by using FBP detection kit (Suobio, Shanghai, China) according to manufacturer's protocols. Briefly, cell and tissue lysates were incubated with 20 μL lysis buffer and reaction reagents sequentially at 37 °C for 1 h, and then the FBP level was quantified by measuring the absorbance of the solution at 540 nm.

2.20. Surface plasmon resonance (SPR)

A Biacore X100 system (GE Healthcare Life Sciences, Marlborough, MA, USA) was used to detect the interaction between PFKL and penfluridol as described previously[16]. Briefly, PFKL protein was immobilized on an active CM7 chip (GE Healthcare Life Sciences). Different concentrations of penfluridol was dissolved in the running buffer and passed over the chip at a certain flow rate, and the K_d value was analyzed.

2.21. Molecular docking

Yinfo Cloud Platform (https://cloud.yinfotek.com) was used to simulate the binding of PFKL and penfluridol according to the instructions. The PFKL protein modeling was obtained from the protein databank (PDB, http://www.rcsb.org).

2.22. Tumor xenograft experiments

Female BALB/c nude mice aged 6−8 weeks were maintained under standard conditions and cared for according to the institutional guidelines for animal care. All the animal experiments were approved by the Ethics Committee for Animal Experiments of Jinan University. ESCC cells resuspended in PBS were mixed with Matrigel (BD Biosciences) in equal volume, then subcutaneously injected into the flanks of nude mice. The tumor size of mice was measured every three days, and tumor volume was calculated using Eq. (1):

$$V = (\text{Length} \times \text{Width}^2)/2 \tag{1}$$

When the diameter of tumors reached ∼5 mm, the mice were divided into different groups for treatment. At the end of experiments, the mice were sacrificed, and the tumors and major organs of mice were collected for further analyses.

2.23. Patient-derived xenograft (PDX) model

The fresh tumor tissues isolated from the ESCC patients were cut into small pieces about 1 mm³ in a sterile environment, and then subcutaneously inoculated into the NOD-*Prkdc*^scid^-*Il2rg*^em1IDMO^ mice (Beijing IDMO Co., Ltd., Beijing, China). Informed consent was obtained from all patients. When the tumor size reached ∼5 mm, the mice were divided into two groups and treated with penfluridol or vehicle, and the tumor size was measured every five days.

2.24. Catalepsy

The duration when animals maintain an imposed position reflects catalepsy and was measured by the high bar test, as previously described[23]. Briefly, the mice were retained in an imposed position with their forelimbs resting on a horizontal bar (diameter: 0.5 cm) that was 4 cm above the benchtop, while their hindlimbs on the benchtop. After the mice were released, the latency they removed both front paws from the bar (*i.e.*, the end point of catalepsy) was videotaped and analyzed by a treatment-blind observer manually.

A mouse is considered cataleptic if it maintains the imposed posture longer than 30 s[24].

2.25. Akinesia

The difficulty for animals in initiating urgent movement reflects akinesia and was assessed with the method as reported before[25,26]. In brief, each mouse was initially acclimatized to the test environment for 5 min on the surface of a wooden elevated platform (length & width: 40 cm; height: 30 cm). The latency of a mouse to move all its four limbs was videotaped and analyzed by a treatment-blind observer manually.

2.26. Locomotor activity

The locomotor activity of mice was determined by the open field test following the routine protocol[27,28]. Briefly, the mice were placed in a noise-free and low-illuminating laboratory environment to acclimatize for 2 h, and then carefully transferred to the center of a plastic arena (length & width & height: 50 cm) divided equally into 25 square zones (10 cm × 10 cm). The trajectory of a mouse was videotaped for 6 min and automatically analyzed with the EthoVision software (Noldus Information Technology, Wageningen, Holland) for locomotor activity-related parameters, including the total moving distance, the mean velocity, and the number of zone-crossing. After each test, the residual odor was removed by 75% ethanol.

2.27. Statistical analysis

The data were expressed as the mean ± SD and significant differences were calculated by t-test. The P values < 0.05 were considered to be significantly different. GraphPad Prism Software 7.0 was used for statistical analyses.

3. Results

3.1. Antipsychotic drug penfluridol exhibits anticancer property in vitro and in vivo

To discover the new indication in oncology of existing drugs, we screened a small molecule library consisting of 1320 FDA-approved drugs. ESCC cells were treated with the 1320 compounds individually or DMSO as a control for 48 h, and cell viability was measured to evaluate the effect of small molecule compounds (Fig. 1A, Supporting Infroamtion Table S3). Afterwards, a literature study was conducted on the 44 candidate drugs with significant inhibitory efficiency ($>70\%$) on cancer cell growth (Supporting Inforamtion Table S4). Among the candidate compounds which have rarely been linked to cancer treatment but exerted strong anticancer bioactivity in our screening assay, penfluridol, a first-generation diphenylbutylpiperidine antipsychotic, drew out great attention and became the focus of this study (Fig. 1B). In order to verify the anticancer property of penfluridol, KYSE30, KYSE150 and KYSE270 cells were treated with different concentrations of penfluridol (up to 10 μmol/L) for 24, 48 and 72 h, respectively. As shown in Fig. 1C, penfluridol inhibited the proliferation of ESCC cells in a dose- and time-dependent manner. The colony formation assay proves that the ability of ESCC cells to form colonies were significantly weakened by penfluridol (Supporting Informaiton Fig. S1A). We also performed annexin V-FITC/PI staining on the cells treated with penfluridol, and the results show that penfluridol induced apoptosis of ESCC cells in a dose-dependent manner (Fig. 1D), which was also evidenced by increased expression level of cleaved caspase-3 (Fig. 1E). Furthermore, we determined whether penfluridol could exhibit anticaner bioactivity in other cancers. The results from WST-1 and colony formation assays show that penfluridol significantly inhibited cell proliferation in colorectal cancer and liver cancer (Fig. S1B and S1C).

We next examined the therapeutic potential of penfluridol in ESCC treatment in animals. Tumor xenografts were established by subcutaneously injecting KYSE270 cells into flanks of nude mice, and the mice were treated with penfluridol or vehicle control. As shown in Supporting Information Fig. S2A, penfluridol treatment led to a significant decrease of tumor volume in a dose-dependent manner, with decreases of 47.1% and 62.1% in the groups receiving 9 and 18 mg/kg of penfluridol, respectively, twice a week. This was confirmed by reduced Ki-67 proliferation index in penfluridol-treated tumors (Fig. S2B). More importantly, when the dosage was reduced to 18 mg/kg once a week, which is equal to the dosage for treatment of schizophrenia in humans, penfluridol also significantly inhibited the growth of tumor xenografts derived from KYSE30 and KYSE270 cells, respectively (Fig. 1F). The Ki-67 immunohistochemical staining and the changes of cleaved caspase-3 indicated that penfluridol induced apoptosis and suppressed tumor cell proliferation (Fig. 1G and H). No significant change in body weight of mice was observed in the treatment group, compared with the control group (Fig. S2C). Penfluridol treatment did not exert toxic effects on the vital organs of mice, indicated by histological examination of liver, kidney, and lung (Fig. S2D). To ensure the safety of penfluridol application in the current study, we conducted several behavioral tests to assess catalepsy, akinesia, and locomotor activity between the drug-treated and the control mice. As shown in Fig. S2E, the latency to the end of catalepsy, the latency to initiate urgent movement, and the locomotor activity were comparable between the two groups. These results suggest that applying penfluridol with the designated protocol did not elicit significant effect on behavioral phenotypes in mice. Collectively, our data reveal that antipsychotic drug penfluridol is a potential anticancer agent.

3.2. Penfluridol inhibits glycolysis in ESCC cells

Different from normal differentiated cells, which depend on the oxidative phosphorylation to provide energy, cancer cells prefer to aerobic glycolysis[29]. To determine the effect of penfluridol on glycolysis, the Seahorse glycolytic rate assay was performed in KYSE150 and KYSE270 cells treated with penfluridol. As shown in Fig. 2A, penfluridol markedly repressed the glycolysis and glycolytic capacity of KYSE150 and KYSE270 cells, reflected by ECAR, whereas only exerted a relatively moderate effect on oxidative phosphorylation, indicated by OCR assay (Supporting Information Fig. S3). Moreover, the glucose consumption and intracellular lactate production were significantly decreased when ESCC cells were exposed to penfluridol (Fig. 2B), and the similar change applied for ATP generation (Fig. 2C).

3.3. IPA uncovers the involvement of AMPK singaling in the anticancer mechanism of penfluridol

To explore the molecular mechanisms how penfluridol inhibits tumorigenesis, RNA-seq was used to compare gene profiles of the
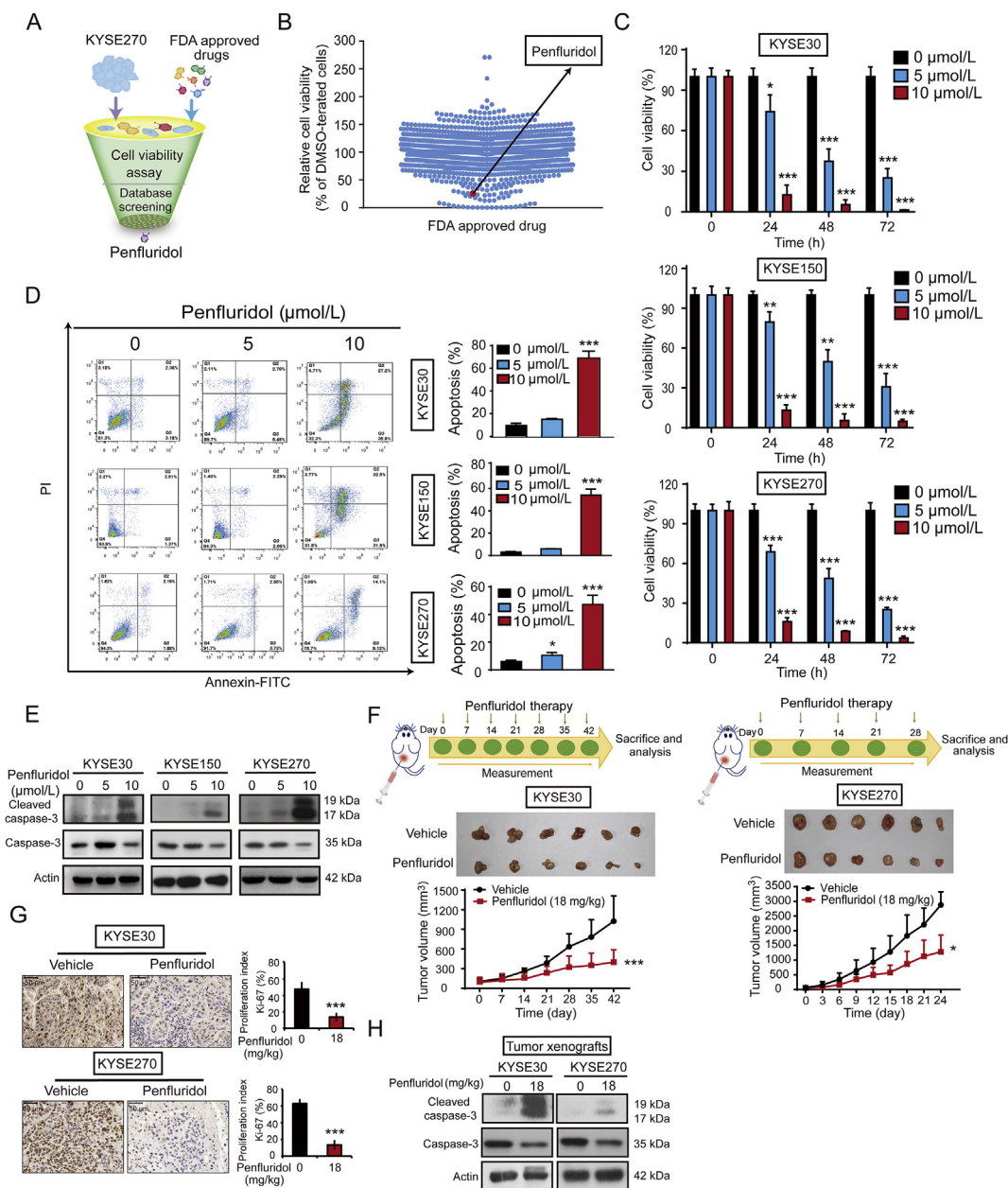
Figure 1 Penfluridol inhibits esophageal squamous cell carcinoma (ESCC) cell proliferation and tumor growth *in vitro* and *in vivo*. (A) Schematic diagram showing the approach to screen the anti-tumor drugs from the US Food and Drug Administration (FDA)-approved small molecule library. (B) KYSE270 cells were treated with 1320 drugs (10 μmol/L) individually for 48 h and subjected to WST-1 assay. (C) Cell viability of KYSE30, KYSE150, KYSE270 cells treated with indicated concentrations of penfluridol (up to 10 μmol/L) was determined. (D) Flow cytometry analysis showing the apoptosis of KYSE30, KYSE150 and KYSE270 cells in the presence of penfluridol. (E) The expression levels of caspase-3 and cleaved caspase-3 were detected in ESCC cells treated with penfluridol. (F) Mice bearing KYSE30-and KYSE270-derived tumor xenografts were given penfluridol (18 mg/kg) once a week ($n = 6$). (G) Penfluridol treatment significantly inhibited Ki-67 proliferation index in KYSE30 and KYSE270 tumor xenografts ($n = 3$). (H) Comparison of cleaved caspase-3 and caspase-3 expression in the KYSE30 and KYSE270 tumor xenografts treated with penfluridol or vehicle by Western blotting. Data are mean ± SD; *$P < 0.05$; **$P < 0.01$; ***$P < 0.001$ compared to control group.

ESCC cells treated with penfluridol (10 μmol/L) and DMSO. A total of 1539 differentially expressed genes were found in penfluridol-treated ESCC cells (fold change > 2, $P < 0.05$), of which 573 were upregulated and 966 were downregulated. IPA was used to analyze the differentially expressed genes to identify the signaling pathways that may be involved in the mechanisms of

action of penfluridol. As shown in Fig. 3A, AMPK signaling, a well-recognized cellular energy sensor which can be activated by energy stress[30], may play an important role in the anticancer bioactivity of penfluridol. The results from Western blotting confirm that penfluridol increased p-AMPK expression, and decreaed expression level of p-p70S6, the downstream molecules
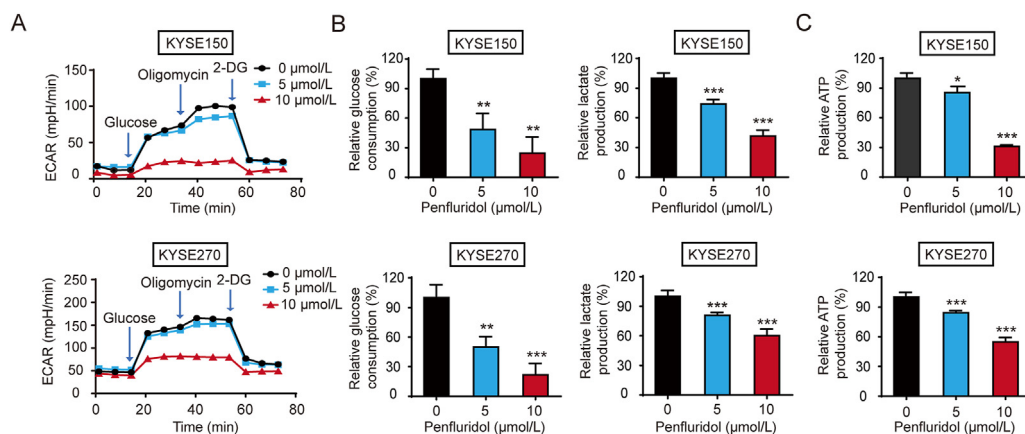
Figure 2 Penfluridol inhibits glycolysis in ESCC cells. (A) Extracellular acidification rate (ECAR) was measured by Seahorse XFe96 analyzer in KYSE150 and KYSE270 cells. (B) and (C) The glucose consumption, and production of lactate and ATP were measured in the presence or absence of penfluridol. Data are mean $\pm$ SD, $n = 3$; *$P < 0.05$; **$P < 0.01$; ***$P < 0.001$ compared to control group.

of AMPK pathway in ESCC cells (Fig. 3B). To investigate the role of glycolysis in AMPK activation, glycolytic inhibitor 2-DG was used in ESCC cells. The WST-1 and Western blotting assays indicated that 2-DG induced the activation of AMPK signaling and suppressed ESCC cell proliferation (Fig. 3C and D). To determine whether AMPK pathway is responsible for the anti-cancer bioactivity of penfluridol in ESCC, KYSE150 and KYSE270 cells were treated with penfluridol in presence or absence of compound C, a specific AMPK inhibitor. The data from WST-1, Western blotting and flow cytometry assays indicate that the increased apoptosis and decreased proliferation in penfluridol-treated ESCC cells were significantly abrogated by AMPK inhibition (Fig. 3E−G). These findings demonstrate that AMPK plays a critical role in the anticancer bioactivity of penfluridol in ESCC cells.

3.4. Penfluridol activates the AMPK/FOXO3a/BIM signaling to induce apoptosis in ESCC cells

Our Western blotting data show that penfluridol not only induced nuclear accumulation of FOXO3a (Fig. 4A), a downstream target of AMPK pathway[31,32], but also induced expression of BIM, a proap-optotic protein (Fig. 4B). Since FOXO3a has been reported to function as a transcription factor to activate BIM expression[33,34], we postulated that AMPK/FOXO3a/BIM regulatory axis is required for the anticancer bioactivity of penfluridol. To verify our hypothesis, the subcellular distribution of FOXO3a in ESCC cells was detected by immunofluorescence staining. As shown in Fig. 4C, the nuclear localization of FOXO3a, which was required for its functional role as transcription factor, was increased by penfluridol compared to the control group. In addition, KYSE150 and KYSE270 cells were transfected with the pGL3 plasmid expressing promoter region of BIM, and treated with penfluridol or DMSO control. The results from qRT-PCR and dual luciferase reporter assays showed that penfluridol significantly enhanced the transcriptional activity of BIM promoter and mRNA expression level of BIM in a dose-dependent manner (Fig. 4D and E). Moreover, ChIP assay was performed to verify the binding of FOXO3a to BIM promoter. The results proved that FOXO3a directly binds to BIM promoter, which could be enhanced by penfluridol treatment (Fig. 4F). When the binding sites critical for the interaction between FOXO3a protein and BIM promoter were

mutated (Fig. 4G), penfluridol could not affect the transcriptional activity of BIM promoter (Fig. 4H). Furthermore, the results from WST-1 and Annexin V-FITC/PI staining assays indicated that silencing of FOXO3a with siRNAs signficantly abrogate the effect of penfluridol on apoptosis and proliferation of ESCC cells (Supporting Informaiton Fig. S4). To investigate the role of AMPK in the regu-lation of FOXO3a/BIM axis by penfluridol, immunofluorescence staining and Western blotting were performed to detect subcellular localization of FOXO3a in the ESCC cells treated with penfluridol in presence or absence of compound C. As shown in Fig. 4I and J, in-hibition of AMPK with compound C markedly attenuated the effect of penfluridol on nuclear translocation of FOXO3a. And the results from Western blotting (Fig. 4K) and luciferase reporter assay (Fig. 4L) further confirm that the activation of AMPK by penfluridol enhanced the nuclear accumulation of FOXO3a, transcriptionally increased BIM expression to induce apoptosis. Thererfore, AMPK/FOXO3a/BIM signaling mediates the anticancer effect of pen-fluridol in ESCC cells.

3.5. High expression of PFKL contributes to tumorigenesis and can predict poor prognosis in ESCC

In order to further explore the direct targets of penfluridol in cancer cells, we combined DARTS technology and mass spec-trometry to search for the binding proteins of penfluridol (Fig. 5A). Interestingly, phosphoglycerate mutase 1 (PGAM1), alidoase, fructose-bisphosphate C (ALDOC), PFKL, phospho-glycerate (PGK1), phosphoenolpyruvate carboxykinase 2, and mitochondrial (PCKGM) were identified as putative targets of penfluridol (Fig. 5B). These candidate proteins are important for cancer cell metabolism[10,35−38], which may explain the molec-ular mechanisms how penfluridol inhibits glycolysis in ESCC cells. By using CRISPR/Cas9 technology, we generated the ESCC cell lines deficient in PGAM1, ALDOC, PFKL, PGK1, PCKGM, respectively, and determined their sensitivity to pen-fluridol treatment. Note that penfluridol significantly inhibited cell proliferation in the cells deficient in PGAM1, ALDOC, PGK1, PCKGM, respectively, but could not exhibit its anti-cancer property in the PFKL-knockout ESCC cells (Fig. 5C), indicating that PFKL is required for the anticancer bioactivity of penfluridol.
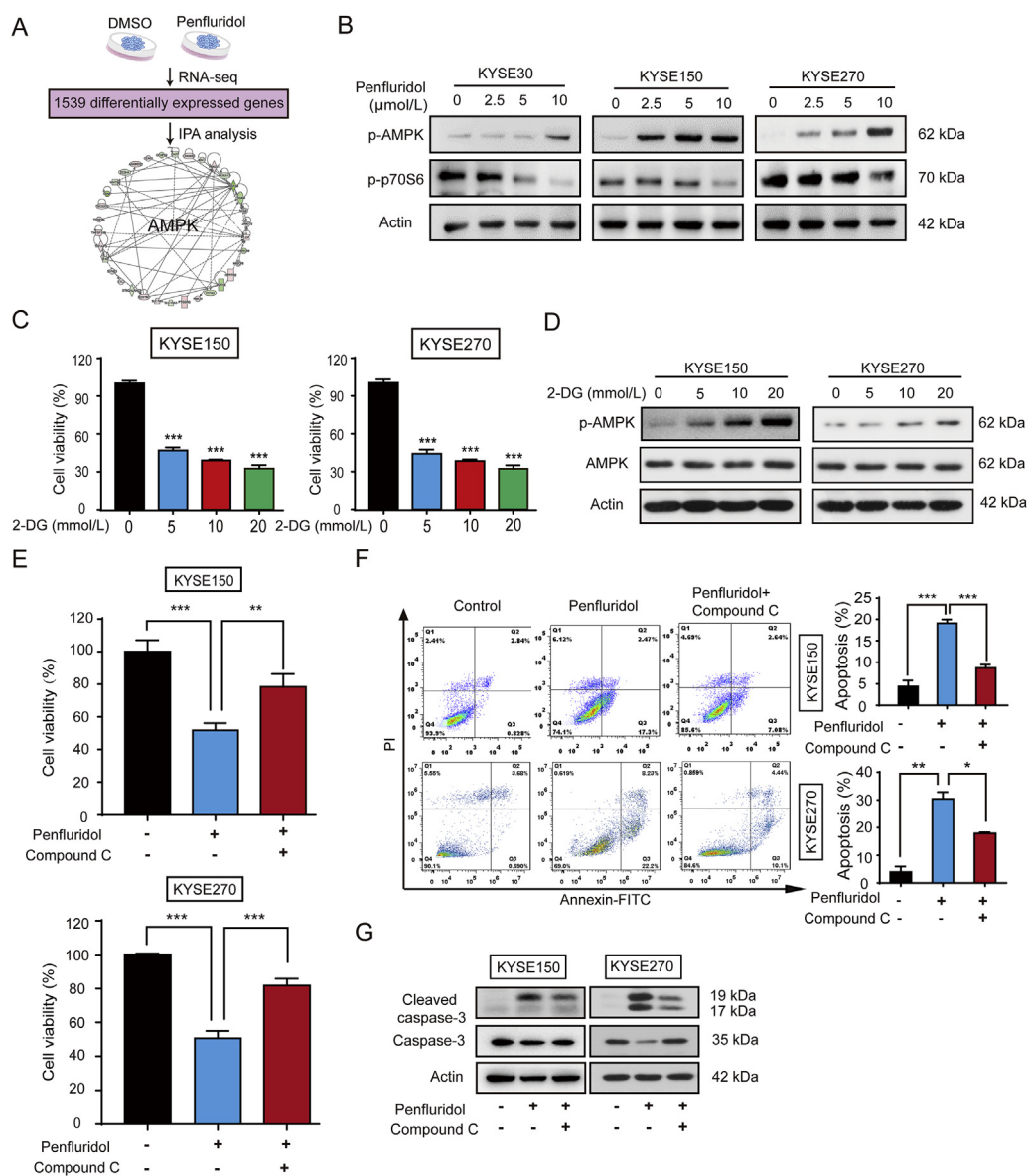
Figure 3 Penfluridol activates AMP-activated protein kinase (AMPK) signaling in ESCC cells. (A) Ingenuity pathway analysis (IPA) suggesting AMPK pathway may be involved in the action mechanism of penfluridol in cancer cells. (B) Western blotting analysis of p-AMPK, and p-p70S6 expression in the KYSE30, KYSE150 and KYSE270 cells treated with different concentrations of penfluridol. (C) and (D) KYSE150 and KYSE270 cells were treated with 2-deoxy-D-glucose (2-DG) (0, 5, 10, and 20 mmol/L) for 24 h, WST-1 assay was taken to measure cell viability (C), and Western blotting was performed to detect expression levels of p-AMPK and AMPK (D). (E)−G) KYSE150 and KTSE270 cells were treated with penfluridol (5 μmol/L) for 48 h in the presence or absence of compound C (0.5 μmol/L), WST-1 assay was taken to measure cell viability (E), flow cytometry analysis was used to determine cell apoptosis (F), and Western blotting was performed to detect expression levels of caspase-3 and cleaved caspase-3 (G). Data are mean ± SD, $n = 3$; *$P < 0.05$; **$P < 0.01$; ***$P < 0.001$ compared to control group.

As one of the rate-limiting enzymes in glycolysis, PFKL plays an important role in cancer progression[3,13], but its biological function and clinical significance in ESCC is unknown. Next, we examined the effect of *PFKL* silencing on ESCC cell proliferation. *PFKL*-deficient stable cell lines, KYSE150-sg*PFKL*#1 and KYSE150-sg*PFKL*#2 as well as KYSE270-sg*PFKL*#1 and KYSE270-sg*PFKL*#2, were established (Fig. 5D). As shown in Fig. 5E and F, the abilities of the *PFKL*-knockout ESCC cells to proliferate and form colonies *in vitro* were markedly inhibited. Moreover, overexpression of PFKL increased cell proliferation in

ESCC cells (Supporting Information Fig. S5A and S5B). To examine the role of PFKL in ESCC tumorigenesis in animals, PFKL-deficient ESCC cells were subcutaneously injected into flanks of nude mice, and found to form smaller tumors than control cells, with decreases of 73.2% and 64.3%, respectively (Fig. 5G). Immunohistochemical staining experiment indicated that the suppressive effect of PFKL silencing on tumorigenesis was attributed to lower Ki-67 cell proliferation index (Fig. 5H).

To study the clinical relevance of PFKL, we detected PFKL expression in a tissue microarray containing 206 cases of ESCC
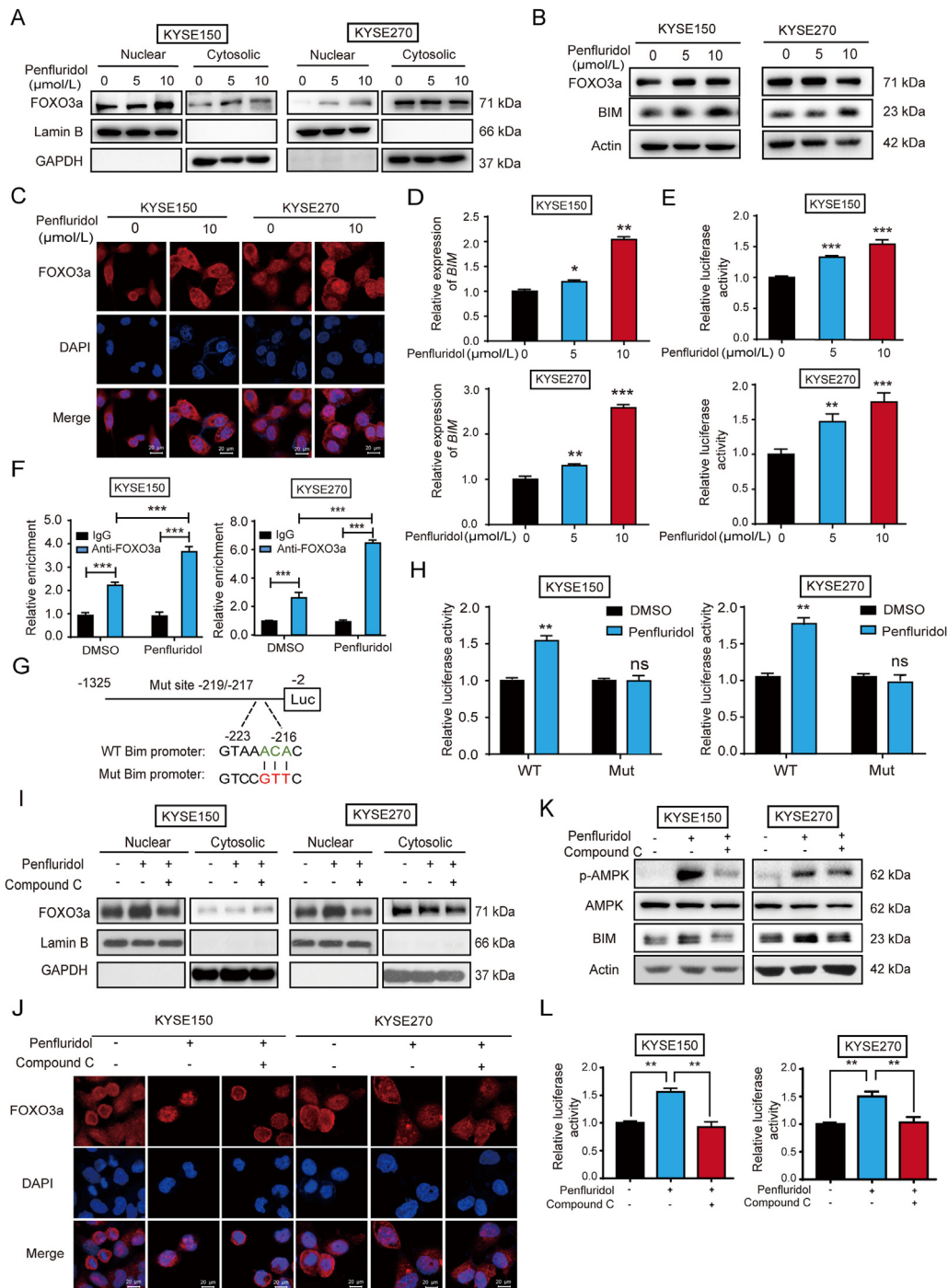
Figure 4 The AMPK/FOXO3a/BIM regulatory axis mediates the anticancer effect of penfluridol. (A) Western blotting analysis of FOXO3a expression in the nuclear and cytoplasmic extracts of ESCC cells, with lamin B and GAPDH as internal controls. (B) KYSE150 and KYSE270 cells were exposed to penfluridol for 24 h, and Western blotting was performed to detect FOXO3a and BIM expression. (C) Immunofluorescent staining showing the subcellular localization of FOXO3a in the presence or absence of penfluridol. (D) The mRNA expression of *BIM* was detected by quantitative real-time polymerase chain reaction (qRT-PCR). (E) The dual luciferase reporter assay showing the effect of penfluridol on luciferase activity of *BIM* promoter in KYSE150 and KYSE270 cells. (F) Chromatin immunoprecipitation (ChIP) assay was used to verify the binding of FOXO3a to *BIM* promoter. (G) The diagram illustrating the mutation design of *BIM* promoter construct. (H) Dual luciferase reporter assay was used to detect the effect of penfluridol on activity of *BIM* promoter in ESCC cells transfected with plasmid expressing wild-type or mutated *BIM* promoter. (I)−(L) KYSE150 and KYSE270 cells were treated with penfluridol in the presence or absence of compound C, subcellular distribution of FOXO3a (I), as well as expression levels of p-AMPK, AMPK and BIM, were determined by Western blotting (K), the subcellular localization of FOXO3a was detected by immunofluorescence (J), and the luciferase activity of *BIM* promoter was measured by dual luciferase reporter (L). Data are mean ± SD, $n = 3$; ns, no significance; *$P < 0.05$; **$P < 0.01$; ***$P < 0.001$ compared to control group.
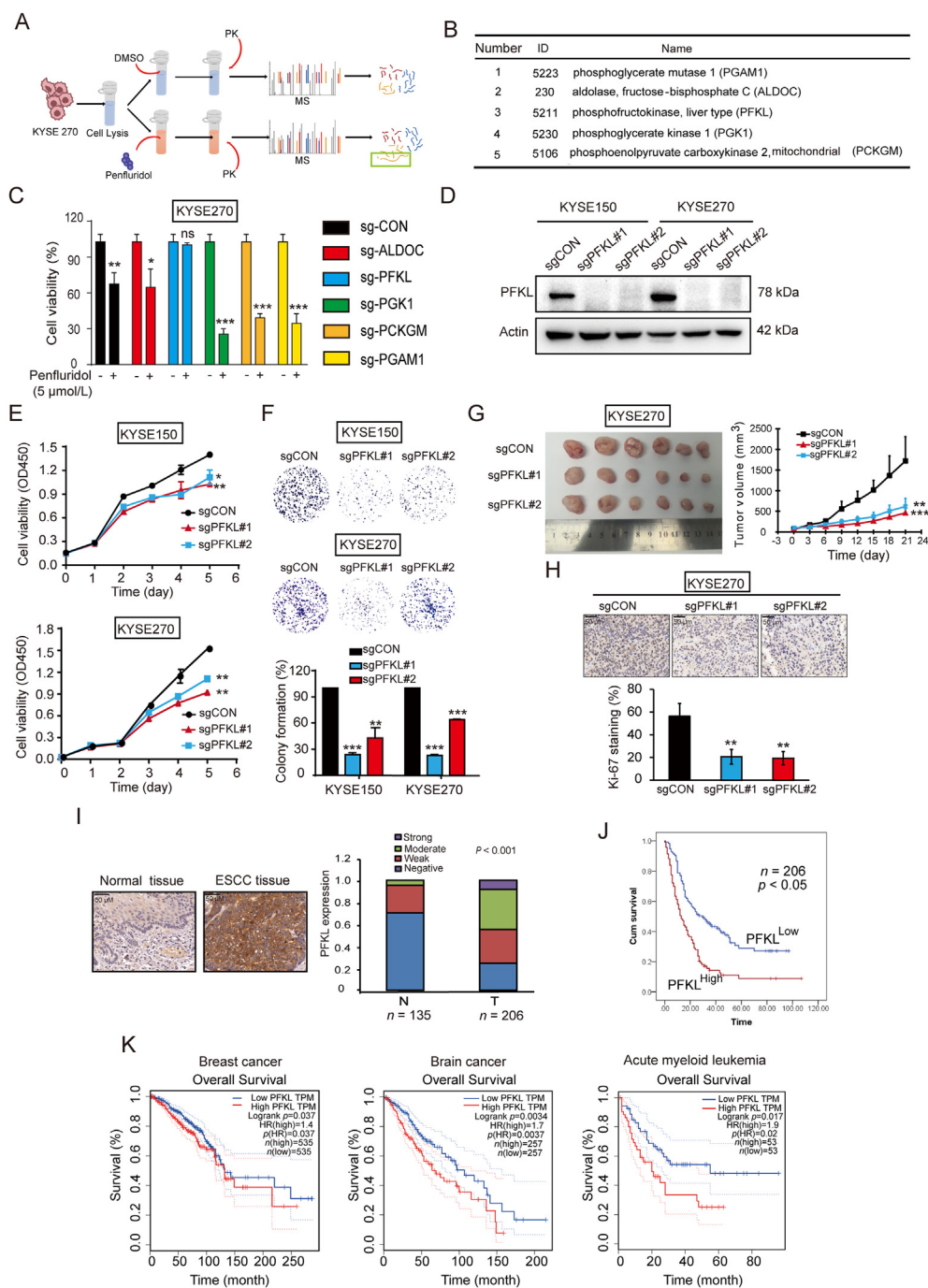
Figure 5 High phosphofructokinase, liver type (PFKL) expression contributes to tumorigenesis and correlates with poor prognosis in ESCC. (A) Schematic diagram showing the drug affinity response target stability (DARTS) technology for identification of the target proteins of penfluridol. (B) Potential target proteins of PFKL identified by DARTS and mass spectrometry. (C) The cell viabilites of penfluridol-treated ESCC cells were determined when the potential target proteins were silenced, including fructose-bisphosphate C (ALDOC), PFKL, phosphoglycerate (PGK1), PCK2 and phosphoglycerate mutase 1 (PGAM1). (D) Successful knockout of PFKL in KYSE150 and KYSE270 cells. (E) and (F) WST-1 and colony formation assays showing the effect of PFKL silencing on ESCC cell proliferation. (G) Tumor growth curves showing the effect of PFKL knockout on growth of ESCC tumor xenografts ($n = 6$). (H) Immunohistochemistry was performed to compare the Ki-67 proliferation index in the tumors among groups ($n = 3$). (I) Representative images of PFKL staining in ESCC tumor and nontumor tissues. (J) Kaplan−Meier analysis showing the suivival of 206 ESCC patients based on tumor PFKL expression. (K) Tumor PFKL expression is correlated with the survival of patients with breast cancer, brain cancer and acute myeloid leukemia. Data are mean $\pm$ SD; ns, no significance; $*P < 0.05$; $**P < 0.01$; $***P < 0.001$ compared to control group.

Table 1 Correlation between PFKL expression levels and clinicopathological parameters in 206 cases of esophageal cancer.

Variable	*n*	Low PFKL	High PFKL	*P* value
Age (years)				
≤55	32	20	12	
>55	174	106	68	0.866
Gender				
Female	46	33	13	
Male	160	93	67	0.094
T-stage				
1/2	37	28	9	
3/4	169	98	71	0.045*
N-stage				
N0	89	66	23	
N1/N2/N3	117	60	57	0.001***
Grade				
I & II	156	102	54	
III & IV	50	24	26	0.028*

*$P < 0.05$; ***$P < 0.001$.

3.6. PFKL is essential for the bioactivity of penfluridol in regulating glycolysis and AMPK/FOXO3a/BIM signaling

We further investigated the importance of PFKL in the inhibitory effect of penfluridol on glycolysis. PFKL-deficient ESCC cells were exposed to penfluridol, and the Seahorse glycolytic rate assay was performed to analyze the changes in ECAR level. Unlike the significant repressive effect in KYSE150 and KYSE270 parental cells as shown in Fig. 2A, no obvious change in the glycolysis and glycolytic capacity was observed when the PFKL-knockout KYSE150 and KYSE270 cells were treated with penfluridol (Fig. 6A). Similarly, penfluridol could not affect the glucose consumption or lactic acid production when PFKL was silenced in ESCC cells (Fig. 6B). These data demonstrate that the PFKL-deficient cells were relatively resistant to penfluridol.

We next studied the function of PFKL in anticancer effect of penfluridol. The results from cell viability and colony formation assays showed that knockout of PFKL markedly weakened the inhibitory effect of penfluridol on ESCC cell proliferation (Fig. 7A and B), whereas overexpression of PFKL had an opposite effect (Fig. S5C and S5D). Annexin V-FITC/PI staining indicated that silencing of PFKL significantly attenuated the effect of penfluridol on ESCC cell apoptosis (Fig. 7C), which was also confirmed by Western blotting analysis of cleaved caspase-3 expression (Fig. 7D). Furthermore, the effect of penfluridol on AMPK/FOXO3a/BIM signaling was determined in PFKL-deficient ESCC cells. As shown in Fig. 7D−F, penfluridol did not cause the activation of AMPK pathway or nuclear accumulation of FOXO3a in KYSE150 and KYSE270 cells when PFKL was silenced. Accordingly, penfluridol treatment did not change the luciferase activity of BIM promoter or the protein expression of BIM (Fig. 7D and G). Together, as a direct target, PFKL mediates the anticancer effect of penfluridol in ESCC.

3.7. Asp-226, Arg-253, and Leu-257 of PFKL are required for anticancer property of penfluridol

PFKL protein was purified and SPR assay was performed to confirm that PFKL is the target of penfluridol *in vitro*. The results from SPR assay show that PFKL can bind to penfluridol with a Kd of 1.4×10^{-8} (Fig. 8A). We next investigated how penfluridol regulates PFKL in ESCC cells, and found that penfluridol had no

tumor tissues and 135 cases of nontumor tissues by immunohistochemistry. As shown in Fig. 5I and 38.8% (80/206) of tumor tissues showed high PFKL expression, whereas only 4.4% (6/135) of nontumor tissues showed high PFKL expression. In contrast, only 61.2% (126/206) of tumor tissues displayed low PFKL expression, whereas 95.6% (129/135) of nontumor tissues showed low PFKL expression. Moreover, PFKL expression was significantly associated with pathologic T stage and tumor grade (Table 1). Kaplan−Meier survival analysis revealed that the patients with high tumor PFKL expression had significantly shorter survival (median survival = 12.0 months) than the patients with lower tumor PFKL expression (median survival = 30.0 months) (Fig. 5J). Analysis of data from the gene expression profiling interaction analysis database confirms that tumor PFKL expression could predict the survival of patients with breast cancer, brain cancer and acute myeloid leukemia[39] (Fig. 5K). Collectively, these data illustrate that PFKL promotes tumorigenesis and is a potential prognostic biomarker in ESCC.
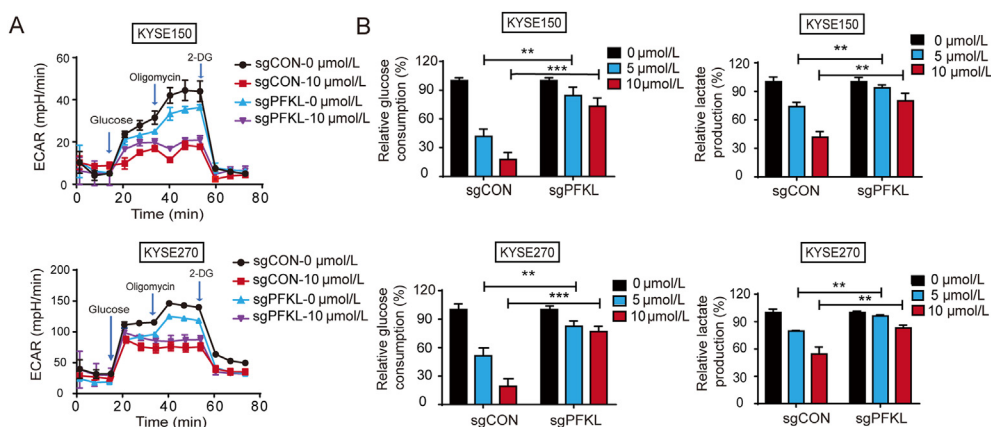

Figure 6 PFKL is important for the function of penfluridol in inhibiting glycolysis. (A) ECAR was measured in the PFKL-deficient KYSE150 and KYSE270 cells treated with penfluridol. (B) Comparison of glucose consumption and lactate production in PFKL-knockout cells exposed to penfluridol. Data are mean ± SD, $n = 3$; **$P < 0.01$; ***$P < 0.001$ compared to control group.
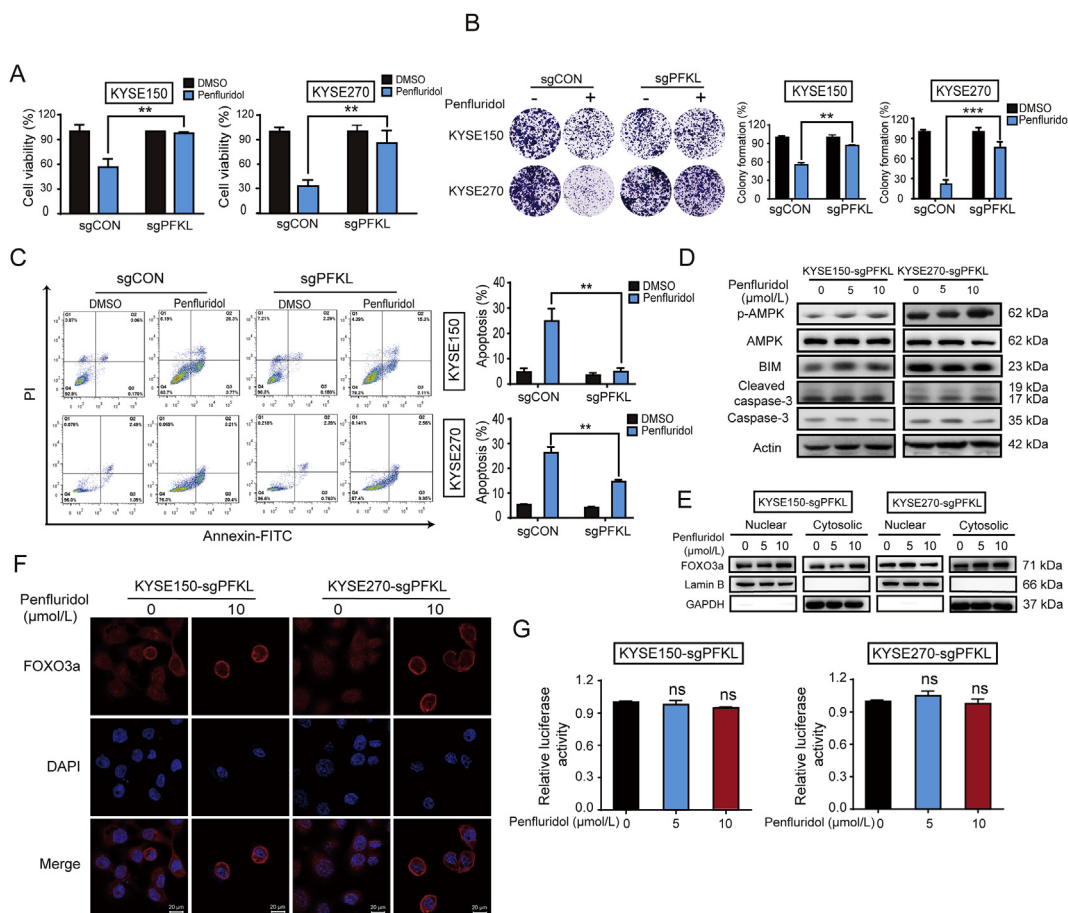
Figure 7 PFKL is required for the bioactivity of penfluridol in regulating AMPK/FOXO3a/BIM signaling and tumorigenesis. (A)–(C) Cell viability assay (A), colony formation assay (B), and flow cytometry analysis (C) were performed to determine the effect of penfluridol on proliferation and apoptosis in PFKL-deficent KYSE150 and KYSE270 cells. (D)–(G) PFKL-deficient KYSE30 and KYSE270 cells were treated with penfluridol, Western blotting (D and E), immunofluorescence (F), and dual luciferase reporter assays (G) were used to detect the subcellular distribution of FOXO3a, expression levels of p-AMPK, AMPK, BIM, cleaved caspase-3, caspase-3, and luciferase activity of *BIM* promoter. Data are mean $\pm$ SD, $n = 3$; ns, no significance; $^{**}P < 0.01$; $^{***}P < 0.001$ compared to control group.

effect on the protein expression of PFKL (Fig. 8B). Since PFKL is a key enzyme in glycolysis, we hypothesized that penfluridol can inhibit glycolysis by affecting the activity of PFKL. The enzyme activity experiment showed that PFKL activity was significantly inhibited in the penfluridol-treated ESCC cells in a dose-dependent manner (Fig. 8C), and the similar results were observed in tumor xenografts (Fig. 8D). During glycolysis, PFKL catalyzes fructose 6-phosphate to FBP (Fig. 8E). Our results show decreased FBP level in penfluridol-treated ESCC cells and tumor xenografts, confirming that penfluricol can inhibit glycolysis in ESCC *in vivo* and *in vitro* (Fig. 8F and G). In addition, we treated KYSE150 and KYSE270 cells with penfluridol in presence or absence of FBP, and determined the cell viability. As shown in Fig. 8H, addition of FBP markedly abrogated the repressive effect of penfluridol on ESCC cell proliferation, which confirmed that inhibited glycolysis in penfluridol-treated cancer cells was attributed to decreased PFKL activity.

Molecular docking was used to predict the binding sites of penfluridol in PFKL, and Thr-193, Gln-197, Asp-226, Arg-253, Leu-257, His-453 and Ala 456 of PFKL are most likely to be required for the binding of penfluridol to PFKL (Fig. 8I). We constructed three plasmids expressing different PFKL mutants,

in which Thr-193 and Gln-197 were mutated and designated as mutant#1, Asp-226, Arg-253 and Leu-257 were mutated and designated as mutant#2, His-453 and Ala-456 were mutated and designated as mutant#3 (Fig. 8J). The PFKL-deficient KYSE150 and KYSE270 cells were overexpressed with wild-type PFKL and three different mutant PFKL, respectively, and treated with penfluridol. The results from WST-1 and colony formation assays show that wild-type PFKL, mutant#1, and mutant#3, but not mutant#2, significantly restored the sensitivity of PFKL-deficient ESCC cells to penfluridol to a level comparable to parental cells (Fig. 8K and Supporting Information Fig. S6A). Furthermore, the important role of PFKL in anticancer property of penfluridol was evaluated in animal model. PFKL-deficient KYSE270 cells and those further re-overexpressed with wild-type and mutant#2 PFKL, respectively, were subcutaneously injected into nude mice to establish tumor xenografts. Each group was divided into two sub-groups and then treated with penfluridol or vehicle. Penfluridol did not inhibit growth of the tumor xenografts derived from *PFKL*-knockout cells. More importantly, the antitumor effect of penfluridol was recovered when the cells were re-overexpressed with wild-type PFKL, but not the mutant#2 (Fig. 8L). Then, the expression of cleaved
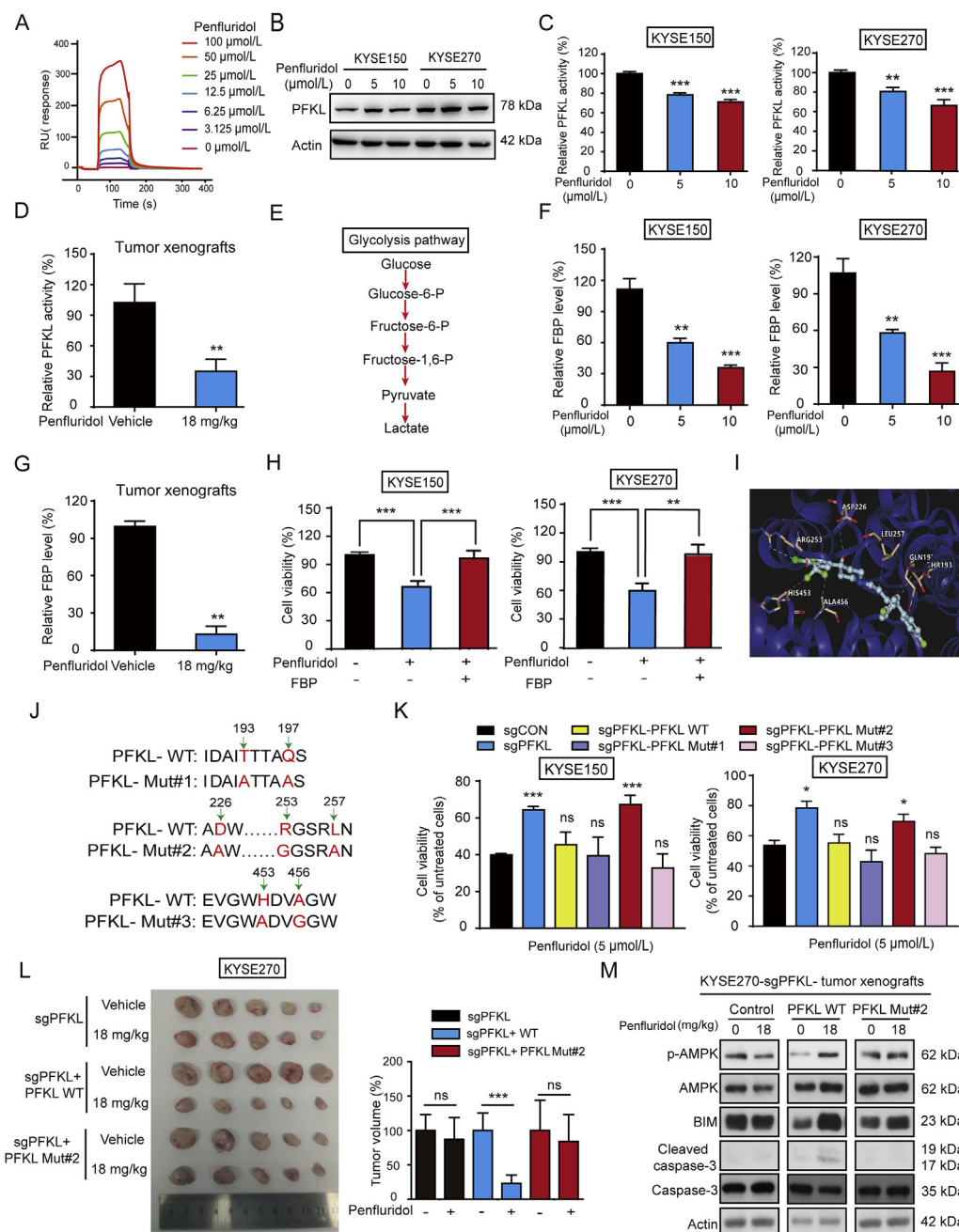
Figure 8 Asp-226, Arg-253, and Leu-257 sites in PFKL are the binding sites required for anticancer bioactivity of penfluridol. (A) Surface plasmon resonance (SPR) result showing that binding of PFKL protein to penfluridol. (B) Western blotting analysis of PFKL expression in KYSE150 and KYSE270 cells treated with penfluridol. (C) Penfluridol inhibited the activity of PFKL in KYSE150 and KYSE270 cells in a dose-dependent manner. (D) Penfluridol inhibited the activity of PFKL in ESCC tumor xenografts ($n = 3$). (E) The diagram showing the process of glycolysis. (F) and (G) Penfluridol reduced fructose 1,6-bisphosphate (FBP) level in ESCC cells (F) and tumor xenografts ($n = 3$) (G). (H) WST-1 assay was used to determine the cell viability in KYSE150 and KYSE270 cells exposed to penfluridiol (5 μmol/L) in the presence or absence of FBP (0.5 μmol/L) for 24 h. (I) The homology modeling structure predicting the binding sites of penfluridol on PFKL protein. (J) Schematic diagram of PFKL mutation. (K) The PFKL-deficient KYSE150 and KYSE270 cells re-overexpressed with the plasmid expressing PFKL-WT, PFKL-Mut#1, PFKL-Mut#2 or PFKL-Mut#3, respectively, were treated with penfluridol for 24 h and cell activity was detected by WST-1 assay. (L) The pictures and tumor volume showing that the antitumor effect of penfluridol was recovered when the PFKL-deficient ESCC cells were re-overexpressed with wild-type PFKL, but not the mutant PFKL ($n = 5$). (M) Western blotting analysis of p-AMPK, AMPK, BIM, cleaved caspase-3, caspase-3 expression in the indicated tumor xenografts treated with penfluridol or vehicle. Data are mean ± SD; ns, no significance; *$P < 0.05$; **$P < 0.01$; ***$P < 0.001$ compared to control group.

caspase-3 and AMPK/FOXO3a/BIM signaling of tumors were detected by Western blotting. As shown in Fig. 8M, penfluridol treatment did not change the expression of cleaved caspase-3 or AMPK/FOXO3a/BIM signaling in the PFKL-deficient KYSE270 cells and the cells re-overexpressing mutant#2 PFKL. To determine which of Asp-226, Arg-253, and Leu-257 was essential for the anticancer effect of penfluridol, we constructed two plasmids expressing PFKL-mut226, in which Asp-226 was mutated, and PFKL-mut253/257, in which Arg-253 and Leu-257 were mutated, respectively. Since the Arg-253, and Leu-257 sites are close to each other, they were mutated in the same plasmid. The data from WST-1 assay show that Arg-253 and Leu-257 were more important for the anticancer bioactivity of penfluridol (Fig. S6B). The finding on the binding sites
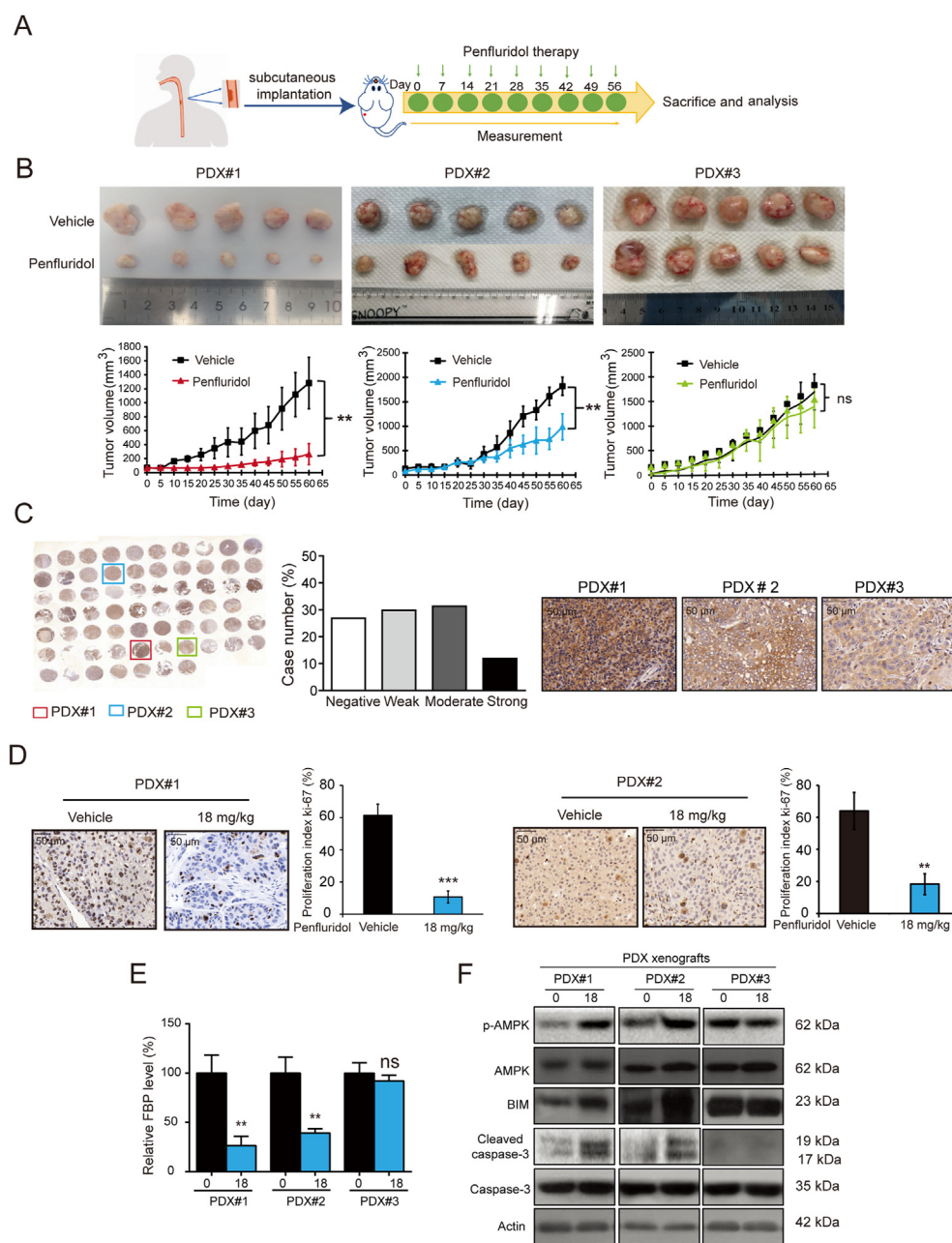

Figure 9 Penfluridol exerts antitumor activity in the Patient-derived xenograft (PDX) models with high PFKL expression. (A) and (B) Three patient-derived xenografts were established in immunodeficient mice, and the mice were given penfluridol (18 mg/kg) or vehicle by oral administration weekly. Penfluridol significantly inhibited the growth of PDX#1 and PDX#2 tumors, but has no effect on PDX#3 ($n = 5$). (C) The expression of PFKL was examined by immunohistochemistry in a tissue microarray consisting of 67 cases ESCC tissues. (D) Quantification of Ki-67 proliferaton index in PDX#1 and PDX#2 tumors ($n = 3$). (E) FBP level in PDX tumors among groups ($n = 3$). (F) Western blot showing the expression of p-AMPK, AMPK, BIM, cleaved caspase-3 and caspase-3 in PDX tumors. Data are mean $\pm$ SD; ns, no significance; **$P < 0.01$; ***$P < 0.001$ compared to control group.

illustrates the pharmacological mechanism of penfluridol, and further provide clues for possible drug reformulation and identification of potential lead compounds with higher treatment efficiency in future.

3.8. Penfluridol exerts strong antitumor activity in the PDX models with high PFKL expression

Three PDX models were established by implanting tumor specimens from ESCC patients into immunodeficient mice (Fig. 9A). As shwon in Fig. 9B, penfluridol significantly inhibited the growth of PDX#1 and PDX#2 tumors, but almost had no effect on PDX#3 tumors. Interestingly, immunohistochemical staining of the three human ESCC specimens, from which the three PDX models were derived, revealed that the tumor#1 and tumor#2 displayed high PFKL expression, but only weak PFKL expression was observed in the tumor#3 (Fig. 9C). This may explain why the PDX models displayed different level of response to penfluridol treatment. We also observed that the proliferation marker Ki-67 in PDX#1 and PDX#2 were obviously decreased by penfluridol (Fig. 9D). We further determined the level of FBP in the PDX tumors and noted that treatment of penfluridol suppressed the glycolysis as shown in Fig. 9E. Moreover, penfluridol treatment resulted in the activation of AMPK signaling, and increased expressions of BIM and cleaved caspase-3 (Fig. 9F). At the same time, penfluridol treatment did not result in toxic effects on liver, lung and kidney of mice (Supporting Information Fig. S7A). Moreover, no significant difference in white blood cells, red blood cells, serum alanine transaminase or aspartate transaminase level was observed in the penfluridol-treated mice (Fig. S7B), suggesting that penfluridol had no side effect on animals.

4. Discussion

Cancer is a disease of tissue growth regulator failure, in this process, cancer cells must overcome enormous energy challenges[40]. As an energy sensor, AMPK is activated to increase ATP production and reduce ATP consumption under cellar energy stress[41]. In this study, we identified penfluridol as a inhibitor of glycolysis, which could reduce glucose consumption and lactate production in cancer cells, leading to the activation of AMPK. The specific inhibitor of AMPK, compound C, significantly weakened the anticancer effect of penfluridol in ESCC cells, consolidating the importance of AMPK signaling pathway in action mechanisms of penfluridol (Fig. 3). FOXO3a, a member of the FOXO subfamily of forkhead transcription factors, plays a critical role in a variety of cellular processes by regulating the expression of downstream target genes[42,43]. The activation of FOXO3a mainly depends on the transport of FOXO3a between nucleus and cytoplasm, which is regulated by a series of phosphatases, such as AKT and AMPK[42]. AMPK activates FOXO3a under conditions of energy stress and regulates the expression of genes including p27 and BIM[42,44]. As one of the BH3-only proteins of BCL-2 family, a subclass of proapoptotic proteins, BIM acts at an apical step to initiate apoptosis[45]. In addition to the fact that BIM expression is downregulated in a variety of tumors[46], BIM-targeting therapies may provide a more effective intervention in cancer management[46]. In this study, we found that penfluridol increased nuclear accumulation of FOXO3a and expression level of BIM, which induced cell apoptosis to suppress tumorigenesis in vitro and in vivo (Fig. 4). These findings not only uncovered the action
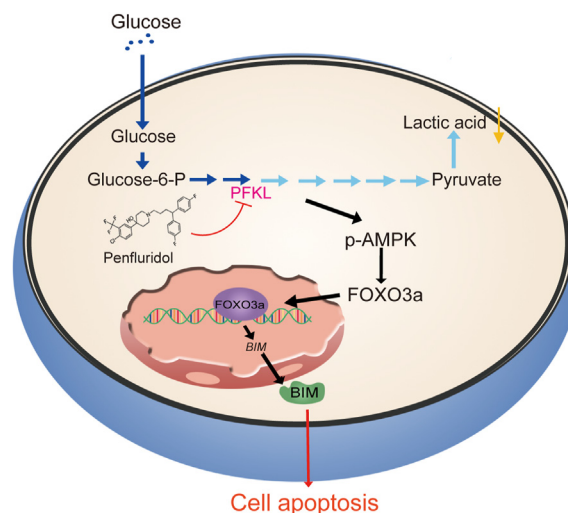

Figure 10 Schematic diagram summarizing how penfluridol suppresses glycolysis and tumorigenesis.

mechanims of penfluridol, but also provided a novel anticancer agent targeting AMPK/FOXO3a/BIM regulatory axis.

Secondly, PFKL was identified as the direct target to mediate the anticancer effect of penfluridol. PFKL is one of the most important rate-limiting enzymes in glycolysis, but its role in human cancer remains to be elucidated, in particular, functional and clinical significance of PFKL in ESCC is unknown. Here, we reported for the first time that PFKL expression is frequently upregulated in tumor tissues, which could predict poor prognosis of the patients with ESCC. The in vitro and in vivo functional assays supported that PFKL contributes to tumorigenesis in ESCC (Fig. 5), suggesting that PFKL is an attracting therapeutic target for cancer treatment. Our findings were corroborated by the recent studies showing that PFKL is upregulated in breast cancer and liver cancer[3], and associated with patient survival[47,48]. In our study, a combination of DARTS technology and mass spectrometry-based proteomics, as well as SPR assay, revealed the direct binding of penfluridol to PFKL. More importantly, based on the molecular docking data, a series of functional and mutagenesis assays demonstrated that penfluridol could not exert is anticancer bioactivity in PFKL-deficient ESCC cells (Figs. 6 and 7). As shown in Fig. 8 and Fig. S6, the Arg-253 and Leu-257 of PFKL are required for the anticancer property of penfluridol. Our findings here provide the first evidence that PFKL contributes to ESCC tumorigenesis and could be a potential therapeutic target in ESCC. More importantly, PFKL protein expression status could be a useful biomarker to stratify ESCC patients for guiding individualized therapy.

According to the global cancer statistics in 2018, the incidence of esophageal cancer ranks seventh, the overall mortality rate ranks sixth worldwide[49]. ESCC is the main histological sub-type of esophageal cancer, and more than 90% of esophageal cancer in China are ESCC[50]. Due to the lack of effective treatment, the five-year survival rate of ESCC patients is less than 20% in developed countriesIn many developing countries where most cases occur, the five-year survival rate is less than 5%[51]. Identification of key oncogenes and screening of therapeutics for treatment of ESCC are urgently needed. Emerging evidences suggest that drug repositioning is a faster and more effective strategy for identification of existing drugs with new indication,

which are safer and have clear descriptions of pharmacokinetics and physicochemical properties. By using phenotypic screening, increasing studies[52,53], including ours[17,18], reported the new indication in oncology of existing drugs. For example, anti-allergic drug azelastine was found to suppress colon tumorigenesis by directly targeting ARF1. In present study, a high-throughput screening was performed in a compound library consisting of 1320 FDA-approved small molecule drugs. Penfluridol, an antipsychotic drug used to treat schizophrenia, was found to exhibit anticancer property *in vitro* and *in vivo*. Our finding was corroborated by another study, which reported that penfluridol could suppress metastatic tumor growth in breast cancer by inhibiting integrin signaling[54]. Mechanistically, penfluridol induces apoptosis to suppress tumorigenesis through inhibition of glycolysis and activation of AMPK/FOXO3a/BIM signaling pathway. More importantly, penfluridol significantly suppressed the growth of PDX tumors, and better response of the PDX tumors to penfluridol treatment was associated with higher PFKL expression in the corresponding tumor specimen, suggesting the implication of PFKL expression as an indicator of drug response for penfluridol treatment in precision medicine.

5. Conclusions

In summary, we performed a high-throughput screening in an FDA-approved drug library consisting of 1320 small molecules, and revealed that penfluridol, a drug to treat schizophrenia in clinic, could suppress ESCC tumor growth *in vitro* and *in vivo*. By integrating DARTS technology, proteomics and SPR assay, we identified PFKL as a direct target of penfluridol. We reported for the first time that PFKL contributes to tumorigenesis and is required for the anticancer bioactivity of penfluridol. Mechanistically, direct binding of penfluridol and PFKL inhibits glycolysis to activate AMPK/FOXO3a/BIM signaling, therefore suppressing tumorigenesis (Fig. 10). Taken together, PFKL may be a promising prognostic biomarker and therapeutic target in ESCC, and our study provides a preclinical rationale for development of penfluridol as a potential drug for the treatment of ESCC.

Author contributions

Cancan Zheng and Xiaomei Yu: acquisition of data, analysis and interpretation of data, statistical analysis, drafting of the manuscript; Yiyao Liang, Yidong Zhu, Yan He, Long Liao, Dingkang Wang, Yanming Yang and Ang Li: acquisition of data, analysis and interpretation of data; Xingfeng Yin: technical and/or material support; Qingyu He and Bin Li: funding acquisition, study concept and design, study supervision.

Conflicts of interest

The authors declare no competing interests.

Appendix A. Supporting information

Supporting data to this article can be found online at https://doi.org/10.1016/j.apsb.2021.09.007.

References

1. Morandi A, Indraccolo S. Linking metabolic reprogramming to therapy resistance in cancer. *Biochim Biophys Acta Rev Cancer* 2017; **1868**:1−6.

2. Koppenol WH, Bounds PL, Dang CV. Otto Warburg's contributions to current concepts of cancer metabolism. *Nat Rev Cancer* 2011;**11**: 325−37.

3. Feng Y, Zhang Y, Cai Y, Liu R, Lu M, Li T, et al. A20 targets PFKL and glycolysis to inhibit the progression of hepatocellular carcinoma. *Cell Death Dis* 2020;**11**:89.

4. Zhao Y, Hu X, Liu Y, Dong S, Wen Z, He W, et al. ROS signaling under metabolic stress: cross-talk between AMPK and AKT pathway. *Mol Cancer* 2017;**16**:79.

5. Gwinn DM, Shackelford DB, Egan DF, Mihaylova MM, Mery A, Vasquez DS, et al. AMPK phosphorylation of raptor mediates a metabolic checkpoint. *Mol Cell* 2008;**30**:214−26.

6. An Y, Wang B, Wang X, Dong G, Jia J, Yang Q. SIRT1 inhibits chemoresistance and cancer stemness of gastric cancer by initiating an AMPK/FOXO3 positive feedback loop. *Cell Death Dis* 2020;**11**:115.

7. Liu Z, Shi Z, Lin J, Zhao S, Hao M, Xu J, et al. Piperlongumine-induced nuclear translocation of the FOXO3A transcription factor triggers BIM-mediated apoptosis in cancer cells. *Biochem Pharmacol* 2019;**163**:101−10.

8. Lomenick B, Hao R, Jonai N, Chin RM, Aghajan M, Warburton S, et al. Target identification using drug affinity responsive target stability (DARTS). *Proc Natl Acad Sci U S A* 2009;**106**:21984−9.

9. Pai MY, Lomenick B, Hwang H, Schiestl R, McBride W, Loo JA, et al. Drug affinity responsive target stability (DARTS) for small-molecule target identification. *Methods Mol Biol* 2015;**1263**:287−98.

10. Li L, Li L, Li W, Chen T, Bin Z, Zhao L, et al. TAp73-induced phosphofructokinase-1 transcription promotes the Warburg effect and enhances cell proliferation. *Nat Commun* 2018;**9**:4683.

11. Yalcin A, Telang S, Clem B, Chesney J. Regulation of glucose metabolism by 6-phosphofructo-2-kinase/fructose-2,6-bisphosphatases in cancer. *Exp Mol Pathol* 2009;**86**:174−9.

12. Nakajima H. Phosphofructokinase (PFK). *Nihon Rinsho* 1995;**53**: 1241−6.

13. Yang J, Li J, Le Y, Zhou C, Zhang S, Gong Z. PFKL/miR-128 axis regulates glycolysis by inhibiting AKT phosphorylation and predicts poor survival in lung cancer. *Am J Cancer Res* 2016;**6**:473−85.

14. Zheng J, Luo J, Zeng H, Guo L, Shao G. [125]I suppressed the Warburg effect viaregulating miR-338/PFKL axis in hepatocellular carcinoma. *Biomed Pharmacother* 2019;**119**:109402.

15. Xu WW, Zheng CC, Zuo Q, Li JQ, Hong P, Qin YR, et al. Genome-wide identification of key regulatory lncRNAs in esophageal cancer metastasis. *Signal Transduct Target Ther* 2021;**6**:88.

16. Xu WW, Huang ZH, Liao L, Zhang QH, Li JQ, Zheng CC, et al. Direct targeting of CREB1 with imperatorin inhibits TGFβ2-ERK signaling to suppress esophageal cancer metastasis. *Adv Sci (Weinh)* 2020;**7**:2000925.

17. Hu HF, Xu WW, Li YJ, He Y, Zhang WX, Liao L, et al. Anti-allergic drug azelastine suppresses colon tumorigenesis by directly targeting ARF1 to inhibit IQGAP1−ERK−Drp1-mediated mitochondrial fission. *Theranostics* 2021;**11**:1828−44.

18. Huang XH, Yan X, Zhang QH, Hong P, Zhang WX, Liu YP, et al. Direct targeting of HSP90 with daurisoline destabilizes beta-catenin to suppress lung cancer tumorigenesis. *Cancer Lett* 2020;**489**:66−78.

19. Hu HF, Xu WW, Zhang WX, Yan X, Li YJ, Li B, et al. Identification of miR-515-3p and its targets, vimentin and MMP3, as a key regulatory mechanism in esophageal cancer metastasis:

functional and clinical significance. *Signal Transduct Target Ther* 2020;**5**:271.

20. Xu WW, Li B, Guan XY, Chung SK, Wang Y, Yip YL, et al. Cancer cell-secreted IGF2 instigates fibroblasts and bone marrow-derived vascular progenitor cells to promote cancer progression. *Nat Commun* 2017;**8**:14399.

21. Hong P, Liu QW, Xie Y, Zhang QH, Liao L, He QY, et al. Echinatin suppresses esophageal cancer tumor growth and invasion through inducing AKT/mTOR-dependent autophagy and apoptosis. *Cell Death Dis* 2020;**11**:524.

22. Li B, Xu WW, Guan XY, Qin YR, Law S, Lee NP, et al. Competitive binding between Id1 and E2F1 to Cdc20 regulates E2F1 degradation and thymidylate synthase expression to promote esophageal cancer chemoresistance. *Clin Cancer Res* 2016;**22**:1243−55.

23. Chicca A, Schafroth MA, Reynoso-Moreno I, Erni R, Petrucci V, Carreira EM, et al. Uncovering the psychoactivity of a cannabinoid from liverworts associated with a legal high. *Sci Adv* 2018;**4**:eaat2166.

24. Abdel-Salam OM, El-Sayed El-Shamarka M, Salem NA, El-Din MGA. Effects of *Cannabis sativa* extract on haloperidol-induced catalepsy and oxidative stress in the mice. *EXCLI J* 2012;**11**:45−58.

25. Naskar A, Manivasagam T, Chakraborty J, Singh R, Thomas B, Dhanasekaran M, et al. Melatonin synergizes with low doses of L-DOPA to improve dendritic spine density in the mouse striatum in experimental Parkinsonism. *J Pineal Res* 2013;**55**:304−12.

26. Naskar A, Prabhakar V, Singh R, Dutta D, Mohanakumar KP. Melatonin enhances L-DOPA therapeutic effects, helps to reduce its dose, and protects dopaminergic neurons in 1-methyl-4-phenyl-1,2,3,6-tetrahydropyridine-induced Parkinsonism in mice. *J Pineal Res* 2015;**58**:262−74.

27. Wang P, Liang Y, Chen K, Yau SY, Sun X, Cheng KK, et al. Potential involvement of adiponectin signaling in regulating physical exercise-elicited hippocampal neurogenesis and dendritic morphology in stressed mice. *Front Cell Neurosci* 2020;**14**:189.

28. Greenbaum L, Lifschytz T, Zozulinsky P, Broner EC, Slonimsky A, Kohn Y, et al. Alteration in RGS2 expression level is associated with changes in haloperidol induced extrapyramidal features in a mutant mouse model. *Eur Neuropsychopharmacol* 2012;**22**:379−86.

29. Vander Heiden MG, Cantley LC, Thompson CB. Understanding the Warburg effect: the metabolic requirements of cell proliferation. *Science* 2009;**324**:1029−33.

30. Lin SC, Hardie DG. AMPK: sensing glucose as well as cellular energy status. *Cell Metabol* 2018;**27**:299−313.

31. Li D, Luo L, Xu M, Wu J, Chen L, Li J, et al. AMPK activates FOXO3a and promotes neuronal apoptosis in the developing rat brain during the early phase after hypoxia-ischemia. *Brain Res Bull* 2017;**132**:1−9.

32. Chiacchiera F, Simone C. The AMPK−FoxO3A axis as a target for cancer treatment. *Cell Cycle* 2010;**9**:1091−6.

33. Li C, Xiao XQ, Qian YH, Zhou ZY. The CtBP1−p300−FOXO3a transcriptional complex represses the expression of the apoptotic regulators Bax and Bim in human osteosarcoma cells. *J Cell Physiol* 2019;**234**:22365−77.

34. Sun T, Zhang J, Deng B, Fan X, Long T, Jin H, et al. FOXO1 and FOXO3a sensitize non-small-cell lung cancer cells to cisplatin-induced apoptosis independent of BIM. *Acta Biochim Biophys Sin (Shanghai)* 2020;**52**:1348−59.

35. Sun Q, Li S, Wang Y, Peng H, Zhang X, Zheng Y, et al. Phospho-glyceric acid mutase-1 contributes to oncogenic mTOR-mediated tumor growth and confers non-small cell lung cancer patients with poor prognosis. *Cell Death Differ* 2018;**25**:1160−73.

36. Chang YC, Yang YC, Tien CP, Yang CJ, Hsiao M. Roles of aldolase family genes in human cancers and diseases. *Trends Endocrinol Metab* 2018;**29**:549−59.

37. He Y, Luo Y, Zhang D, Wang X, Zhang P, Li H, et al. PGK1-mediated cancer progression and drug resistance. *Am J Cancer Res* 2019;**9**:2280−302.

38. Vincent EE, Sergushichev A, Griss T, Gingras MC, Samborska B, Ntimbane T, et al. Mitochondrial phosphoenolpyruvate carboxykinase regulates metabolic adaptation and enables glucose-independent tumor growth. *Mol Cell* 2015;**60**:195−207.

39. Tang Z, Li C, Kang B, Gao G, Li C, Zhang Z. GEPIA: a web server for cancer and normal gene expression profiling and interactive analyses. *Nucleic Acids Res* 2017;**45**:W98−102.

40. Li J, Zhong L, Wang F, Zhu H. Dissecting the role of AMP-activated protein kinase in human diseases. *Acta Pharm Sin B* 2017;**7**:249−59.

41. Herzig S, Shaw RJ. AMPK: guardian of metabolism and mitochondrial homeostasis. *Nat Rev Mol Cell Biol* 2018;**19**:121−35.

42. Liu Y, Ao X, Ding W, Ponnusamy M, Wu W, Hao X, et al. Critical role of FOXO3a in carcinogenesis. *Mol Cancer* 2018;**17**:104.

43. Cao MQ, You AB, Zhu XD, Zhang W, Zhang YY, Zhang SZ, et al. miR-182-5p promotes hepatocellular carcinoma progression by repressing FOXO3a. *J Hematol Oncol* 2018;**11**:12.

44. Farhan M, Wang H, Gaur U, Little PJ, Xu J, Zheng W. FOXO signaling pathways as therapeutic targets in cancer. *Int J Biol Sci* 2017;**13**:815−27.

45. Czabotar PE, Colman PM, Huang DC. Bax activation by BIM?. *Cell Death Differ* 2009;**16**:1187−91.

46. Akiyama T, Dass CR, Choong PF. BIM-targeted cancer therapy: a link between drug action and underlying molecular changes. *Mol Cancer Ther* 2009;**8**:3173−80.

47. Zancan P, Sola-Penna M, Furtado CM, Da Silva D. Differential expression of phosphofructokinase-1 isoforms correlates with the glycolytic efficiency of breast cancer cells. *Mol Genet Metab* 2010;**100**:372−8.

48. Zhang X, Wang J, Zhuang J, Liu C, Gao C, Li H, et al. A novel glycolysis-related four-mRNA signature for predicting the survival of patients with breast cancer. *Front Genet* 2021;**12**:606937.

49. Bray F, Ferlay J, Soerjomataram I, Siegel RL, Torre LA, Jemal A. Global cancer statistics 2018: GLOBOCAN estimates of incidence and mortality worldwide for 36 cancers in 185 countries. *CA Cancer J Clin* 2018;**68**:394−424.

50. Lu Z, Ren Y, Yang L, Jia A, Hu Y, Zhao Y, et al. Inhibiting autophagy enhances sulforaphane-induced apoptosis *via* targeting NRF2 in esophageal squamous cell carcinoma. *Acta Pharm Sin B* 2021;**11**:1246−60.

51. Codipilly DC, Qin Y, Dawsey SM, Kisiel J, Topazian M, Ahlquist D, et al. Screening for esophageal squamous cell carcinoma: recent advances. *Gastrointest Endosc* 2018;**88**:413−26.

52. Moffat JG, Rudolph J, Bailey D. Phenotypic screening in cancer drug discovery-past, present and future. *Nat Rev Drug Discov* 2014;**13**:588−602.

53. Jiang YY, Lin DC, Mayakonda A, Hazawa M, Ding LW, Chien WW, et al. Targeting super-enhancer-associated oncogenes in oesophageal squamous cell carcinoma. *Gut* 2017;**66**:1358−68.

54. Ranjan A, Gupta P, Srivastava SK. Penfluridol: an antipsychotic agent suppresses metastatic tumor growth in triple-negative breast cancer by inhibiting integrin signaling axis. *Cancer Res* 2016;**76**:877−90.